ELSEVIER

Journal of Structural Geology 28 (2006) 1–8

JOURNAL OF STRUCTURAL GEOLOGY

www.elsevier.com/locate/jsg

A rapid method for strain estimation from flattened parallel folds

Deepak C. Srivastava*, Jyoti Shah

Department of Earth Sciences, IIT Roorkee, Roorkee 247667, India

Received 11 May 2005; received in revised form 2 September 2005; accepted 12 September 2005
Available online 2 November 2005

Abstract

Superimposition of homogeneous strain on parallel folds is a potential mechanism for development of flattened parallel folds. Estimation of flattening strain by existing graphical approaches requires a large number of angular and/or linear measurements. We propose a new computer-based approach, which rapidly destrains a flattened parallel fold into a parallel fold with help of any of the commonly available graphic software. This method is based on the principle that the magnitude of flattening directly relates to change in the inherent orthogonality that exists between a tangent and an isogon, at any given angle of the limb dip, on the profile of a parallel fold.

Using six examples of flattened parallel folds, we show that the results of our destraining method are consistent with those yielded by other existing methods. Besides estimating the flattening strain rapidly and involving a relatively low amount of error, our method also restores the pre-flattening fold shape without any additional geometrical or numerical operation.

Keywords: Flattening; Parallel fold; Flattened parallel fold; Oblique-flattening; Fold analysis; Destraining

1. Introduction

Structural geologists have long recognized the significance of geometric analysis of folds because it provides important clues to the mechanism of folding (Ramsay, 1967, pp. 386–411; Hudleston, 1973a; Bastida et al., 2003), besides defining the precise shapes of the fold hinge zones that commonly host petroleum reservoirs and saddle-reef ore bodies. Buckling of a relatively competent layer, enclosed in an incompetent medium, produces class 1B, or parallel folds (Biot, 1961; Ramberg, 1963; Ramsay, 1967, pp. 372–377; Ghosh, 1993, pp. 252–264). These folds are characterized by a unique orthogonal relationship between the tangent and the isogon at any given angle of the limb dip. Flattening, caused by the superimposition of a homogeneous strain on a class 1B fold, results in thickening of the hinge zone, thinning of the limbs and modification of the fold shape into class 1C geometry. The extent of geometrical modification due to flattening is directly related to the magnitude of the superimposed homogeneous strain.

Several graphical methods are available for the determination of magnitude of flattening. Ramsay (1962, 1967, p. 413) uses the relationship between the limb dip angle α, and the normalized orthogonal thickness, t'_α, for estimation of flattening in class 1C folds. Hudleston (1973a) proposes a graphical method, which is based on the relationship between the limb dip angle α and, an angle ϕ between the isogon and the normal-to-the-tangent. Lisle (1992) suggests a polar plot between the inverse thickness, $1/t$, and the limb dip angle α, which yields the required strain ellipse. Srivastava (2003) gives a somewhat similar solution, but his method is applicable only to truly concentric folds. None of these existing methods restores the pre-flattening shape of class 1C folds without the application of an additional step that destrains the fold shape either by geometrical or numerical technique.

In this paper, we propose an alternative method for estimation of the flattening strain in class 1C folds. This method, based on destraining by simple computer application, gives the flattening strain and restores the pre-flattening shape of the fold in the same operation. We test the efficacy and the validity of this new method on six examples of natural and numerically simulated folds, and

* Corresponding author. Tel.: +91 1332 285558; fax: +91 1332 273560.
E-mail address: dpkesfes@iitr.ernet.in (D.C. Srivastava).

0191-8141/$ - see front matter © 2005 Elsevier Ltd. All rights reserved.
doi:10.1016/j.jsg.2005.09.001

compare our results with those obtained by other common methods.

2. Destraining method

We assume that the fold to be analyzed develops as a class 1B fold and it assumes class 1C geometry due to superimposition of a post-buckling homogeneous strain ($X \geq Y \geq Z$), albeit a class 1C fold can also develop due to simultaneous buckling and flattening (Hudleston, 1973b).

Our method makes use of two geometrical properties of folds. First, in the class 1B folds, all the isogons are perpendicular to their respective tangents. Second, flattening introduces an angular shear, due to which the orthogonality between the isogons and their corresponding tangents is changed, except at the limb dip, where the isogon and the tangent parallel the principal axes of the strain ellipse. The angle, δ, between the tangent and the isogon at any point in a class 1C fold is a function of the magnitude of flattening, or axial ratio, of the strain ellipse on profile plane. The proposed method destrains a class 1C fold into a class 1B fold by restoring the orthogonal relationship between isogons and their respective tangents. The ratio, arc length/half wavelength, measured on the restored fold shape, gives buckling strain R_B, provided the area remains constant during folding. If the initial layer-parallel-shortening is insignificant, then the estimate of bulk strain, R_{Total}, can be made by multiplying the strains due to buckling and flattening, i.e. $R_{Total} = R_B R_F$.

2.1. Application

The destraining of class 1C fold, based on the principle of restoring orthogonal relationship between isogons and their respective tangents, is best applied using any common graphic software, e.g. CorelDRAW, Corel Photo-Paint, Adobe Illustrator or Smartdraw. The two limbs of any given fold can be analyzed together, or separately, depending upon the presence, or the lack, of perfect mirror image symmetry across the axial trace. We first consider a simple situation where the *X–Z* plane is profile plane and the *X*-axis parallels axial trace on profile plane of class 1C fold. These simplifying assumptions are realistic because many natural examples of the class 1C folds show a parallelism between axial trace and cleavage trace on profile plane. These class 1C folds, characterized by the orthogonal relationship between the isogon and the tangent at hinge points, can be destrained as follows:

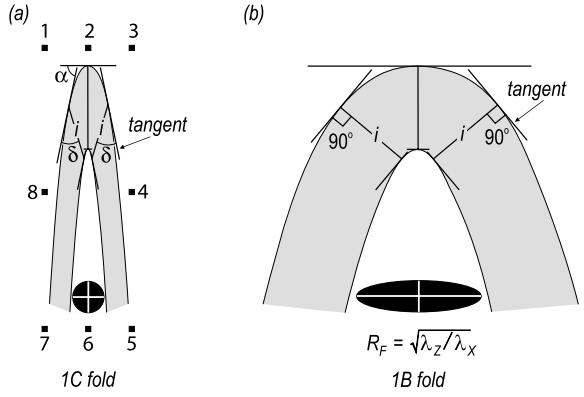

Fig. 1. Destraining methodology. (a) Image of a class 1C fold, and a reference circle. δ—angle between isogon (i) and tangent at any given angle of the limb dip (α). Selection of these objects displays a set of eight handles as the squares, *1–8*. (b) Destraining is achieved by pulling the handle-*4* towards the right until the orthogonal relationship between isogons and their respective tangents is restored. The reference circle in (a) transforms into the reciprocal strain ellipse of axial ratio R_F in (b). λ_z and λ_x—principal quadratic elongations.

(i) Import the digital or scanned image of profile section of the given fold into a graphic software, say CorelDRAW. Rotate the fold until its axial trace becomes vertical.

(ii) Draw two or three isogons and their respective tangents at convenient angles of the limb dip (Fig. 1a). In principle, only one pair of tangent and isogon at an angle of the limb dip, $90 > \alpha > 0$, is necessary. Also, draw a reference circle near the fold (Fig. 1a).

(iii) Group all objects, namely, the given fold, the tangent lines, the isogons and the circle. Select the grouped objects using the pick tool. This operation displays a set of eight handles, numbered *1–8* in Fig. 1a.

(iv) Drag the handle-*4* horizontally across the axial trace until all the isogons become perpendicular to their respective tangents. The shape of the given fold now restores back to class 1B geometry and the circle, drawn in step-(ii) (Fig. 1a), transforms into the reciprocal strain ellipse of axial ratio $R_F = \sqrt{(\lambda_z/\lambda_x)}$, where λ_z and λ_x are the principal quadratic elongations (Fig. 1b).

Alternatively, the destraining can also be achieved by dragging any one of the handles numbered *2*, *6* or *8* in Fig. 1a.

We now consider the situation of oblique-flattening, where a class 1B fold assumes class 1C geometry due to flattening in such a manner that neither of the principal directions of strain parallels axial trace on profile plane (Hudleston, 1973a; Srivastava and Srivastava, 1988). In such class 1C folds, the isogons and the tangents at the hinge points neither display an orthogonal relationship nor parallel the principal directions of strain. Of the two orthogonal pairs of the isogons and the tangents, which may occur at limbs of the obliquely-flattened parallel folds (*I–T* and *I′–T′* in Fig. 2a), the identification of any one pair is sufficient for knowing the principal directions of strain. The procedure for the estimation of flattening strain and the restoration of

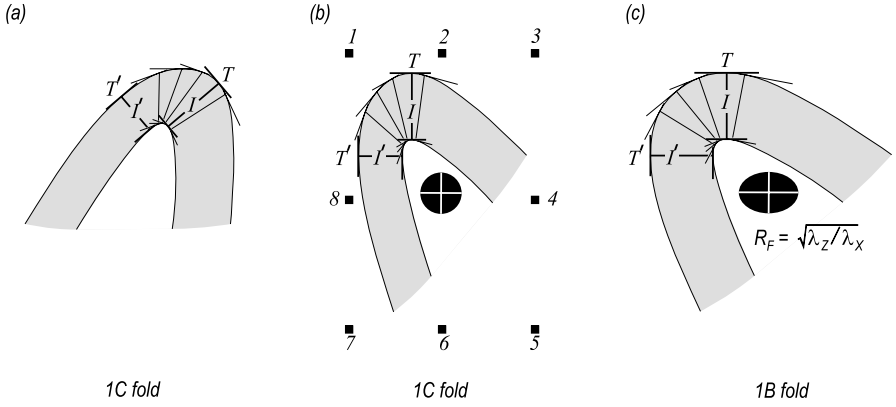

Fig. 2. (a) Profile section of an obliquely-flattened class 1C fold along with isogon–tangent pairs at different points. The two isogon–tangent pairs, *I*–*T* and *I*′–*T*′, showing orthogonal relationships, parallel the principal directions of strain. (b) *I* is made vertical by rotating the objects in (a). Circle—reference circle. Black squares—eight handles, *1*–*8*, which appear on selection of the grouped objects. (c) Restored fold of class 1B geometry. R_F—axial ratio of the reciprocal strain ellipse.

pre-flattening shape of obliquely-flattened parallel folds is as follows:

(i) Import the image of profile section of the given class 1C fold into a graphic software, e.g. CorelDRAW, and draw isogon–tangent pairs at different angles of the limb dip on both limbs. Decipher principal directions of the flattening strain along the isogon and the tangent that exhibit an orthogonal relationship (*I*–*T* and *I*′–*T*′ in Fig. 2a). Draw a reference circle near the fold. Group and rotate these objects to make the isogon, *I*, or the isogon *I*′ vertical (Fig. 2b).

(ii) Use the pick tool and select the grouped objects to display eight handles, namely, *1*–*8* in Fig. 2b. Drag the handle-*4* towards right until all the isogons retrieve perpendicular relationship with their respective tangents (Fig. 2c). Alternatively, the orthogonal relationship between isogons and their respective tangents can also be retrieved by dragging any one of the handles numbered *2*, *6* or *8* in Fig. 2b. This operation restores the class 1B geometry of the fold and transforms the reference circle into the reciprocal ellipse of axial ratio, $R_F = \sqrt{(\lambda_z/\lambda_x)}$.

3. Examples

The proposed destraining method is tested on the profile sections of a large number of published and unpublished folds. Four examples of natural folds presented here are: (i) a reclined fold, plunging at 60° towards NNW, and traced by an aplite vein in the Precambrian migmatite complex near Masuda (N26°07′: E74°32′), northwestern India (Fig. 3a), (ii) a fold in the sandstone layer, enclosed in the shale beds in the Proterozoic Vindhyan sedimentary sequence, exposed near Bassi Railway station (N25°01′: E74°45′), northwestern India (Fig. 3b). This fold plunges at 30° towards

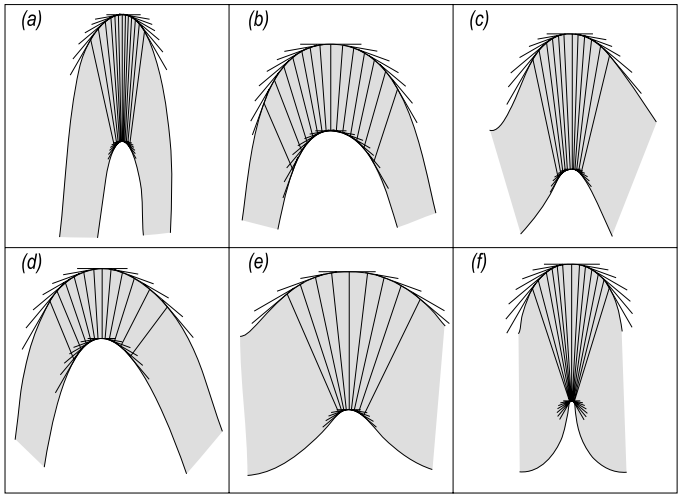

Fig. 3. Isogons and tangents on the profile sections of the six folds tested in this study. (a)–(d) Natural folds. (e) and (f) Computer simulated folds.

327° and its axial plane dips at 76° towards 246°, (iii) a part of the folded pegmatite vein in the pelitic Moine rocks, Scotland (Fig. 3c taken from fig. 11A in Hudleston (1973c)), and (iv) antiformal part of the fold in the Precambrian gneisses of Gjeroy, Nordland, Norway (Fig. 3d taken from fig. 2 in Lisle (1992)). In addition to these four examples of natural folds, we have also tested the efficacy of the new method on two computer-simulated folds (Fig. 3e and f) taken from fig. 6A and B in Dietrich (1969).

In the most comprehensive account of fold analysis published to date, Hudleston (1973c) shows that the magnitude of flattening on opposite limbs of folds could be somewhat different (Treagus and Treagus, 1981; Treagus, 1982). To minimize errors that may arise due to the inhomogeneity in flattening strain in different parts of folds, we analyze the left and right limbs of each fold separately. The magnitude of flattening strain, expressed in terms of axial ratio of the strain ellipse, and the pre-flattening shapes of left and right limbs in each fold are shown in Fig. 4a–f. For a critical comparison of the different methods, the six folds treated by the destraining technique are also analyzed by the $t'_\alpha - \alpha$, the ϕ–α, and the inverse thickness methods (Figs. 5–7). As shown in Table 1, results obtained by the destraining technique are consistent with the solutions yielded by other methods.

4. Discussion

Similar to other existing methods for estimation of the flattening strain, our method, too, is best suited to those class 1C folds that evolve by superimposition of flattening over buckling (Ramsay, 1967, p. 411). Soft model experiments by Hudleston (1973b) demonstrate that simultaneous buckling and flattening is also an efficient mechanism for the development of class 1C folds, particularly in situations where the initial wavelength of folds is much larger than the wavelength predicted by buckling equations and the viscosity contrast is very low (Ramberg, 1963). The $t'_\alpha - \alpha$ and the ϕ–α curves for the class 1C folds developed by simultaneous buckling and flattening and those formed by superimposition of flattening over buckling are, however, similar, except at steep angles of the limb dip (fig. 11D and E in Hudleston, 1973b; Treagus, 1982). Application of Ramsay's $t'_\alpha - \alpha$ and Hudleston's ϕ–α curves on the Class 1C folds, developed by simultaneous buckling and flattening, yields solutions that are either close to, or slight overestimates of, the actual flattening (Chatterjee, 1987). It is evident that the estimates of the strain in those class 1C folds that develop by simultaneous buckling and flattening, e.g. folds in Fig. 3e and f, are at best approximate.

Errors in the $t'_\alpha - \alpha$ and the ϕ–α methods are calculated in

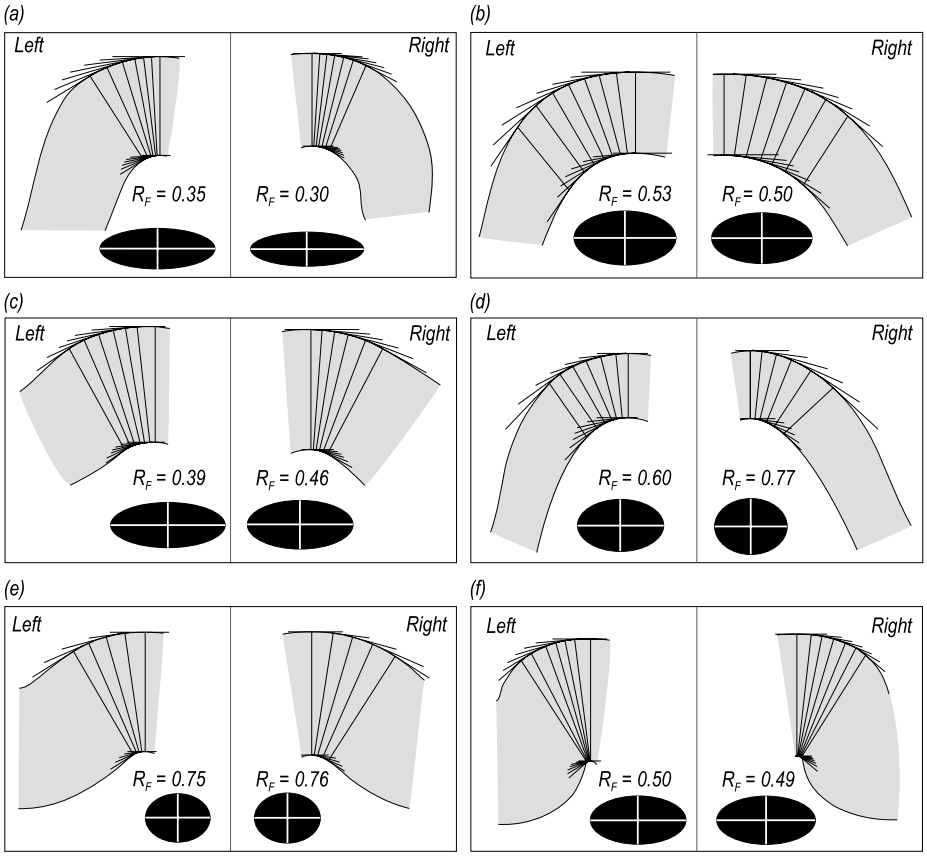

Fig. 4. (a)–(f) Destrained profiles of left and right limbs of six examples of folds shown in Fig. 3a–f, respectively. Note that orthogonality between tangents and respective isogons is restored. Ellipses represent the reciprocal strain ellipse of axial ratio R_F in each case.

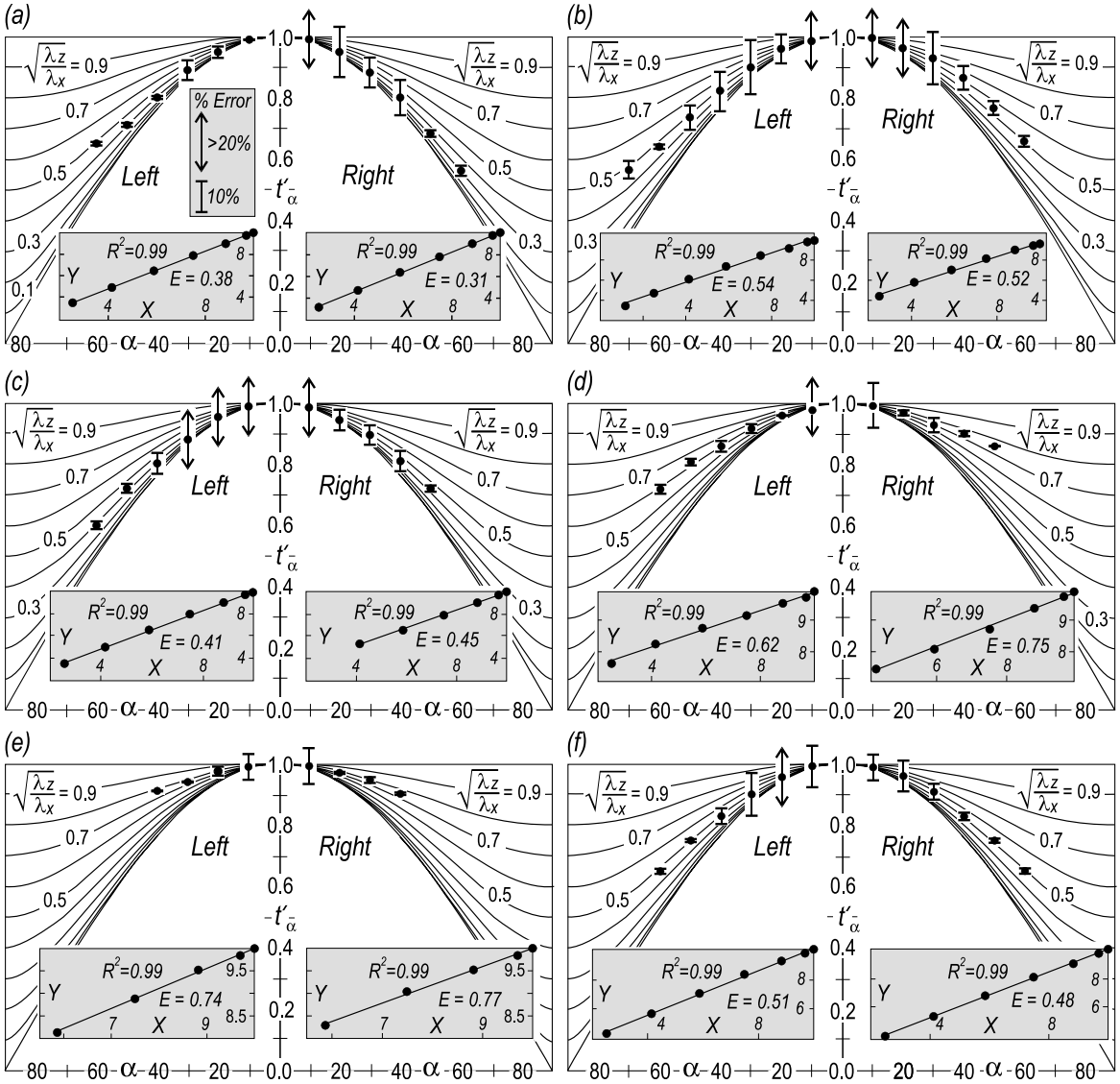

Fig. 5. (a)–(f) $t'_\alpha - \alpha$ plots for left and right limbs of six folds shown in Fig. 3a–f, respectively. Error bars in all the figures are scaled off, as per the %-error scale, shown in (a). Insets show the best-fit lines, obtained by linear transformation of $t'_\alpha - \alpha$ curves. $X = \cos^2\alpha$, $Y = (t'_\alpha)^2$, R^2—regression coefficient. E—expected value of the axial ratio, $\sqrt{(\lambda_z/\lambda_x)}$, given by the square root of the intercept of the best-fit line (Eq. (A2)).

terms of %-error in $\sqrt{(\lambda_z/\lambda_x)}$ ratios at different angles of the limb dip (Appendix). Figs. 5 and 6 show that both the methods, $t'_\alpha - \alpha$ and ϕ–α, tend to produce significant errors, particularly at low ($<15°$) and very steep ($>60°$) angles of the limb dip. There are two potential sources of these errors. First, it is difficult to locate hinge points precisely in many natural folds, and a small shift in location of the hinge points may result in significant errors, particularly at low angles of the limb dip. As our method does not require locating hinge points, it is free from these errors. Second, in many folds, it is difficult to draw the precise tangents at steep angles of the limb dip ($>60°$) due to small changes in curvatures near the inflection points. Owing to these limitations, the $t'_\alpha - \alpha$ and the ϕ–α curves yield optimum solutions by fitting the data points that correspond to the limb dips between 15 and 60°.

Although %-errors in $\sqrt{(\lambda_z/\lambda_x)}$ ratios at individual angles of the limb dip are difficult to calculate in the inverse thickness method, it is evident from Fig. 7 that $1/t - \alpha$ polar plots lie very close to the best-fit ellipse. The inverse thickness method has an additional merit of being independent of the assumption that the direction of maximum elongation parallels the axial trace.

In order to evaluate errors in the destraining method, several pairs of tangent and isogon are drawn on the given class 1C fold (Fig. 3a–f). Because, in practice, all the tangent–isogon pairs may not retrieve the orthogonality at the same amount of destraining, the class 1C folds are destrained to an optimal condition where most isogons approach, or achieve, the orthogonal relationship with their respective tangents (Fig. 4a–f). Errors in destraining method can now be evaluated in terms of an estimator, namely,

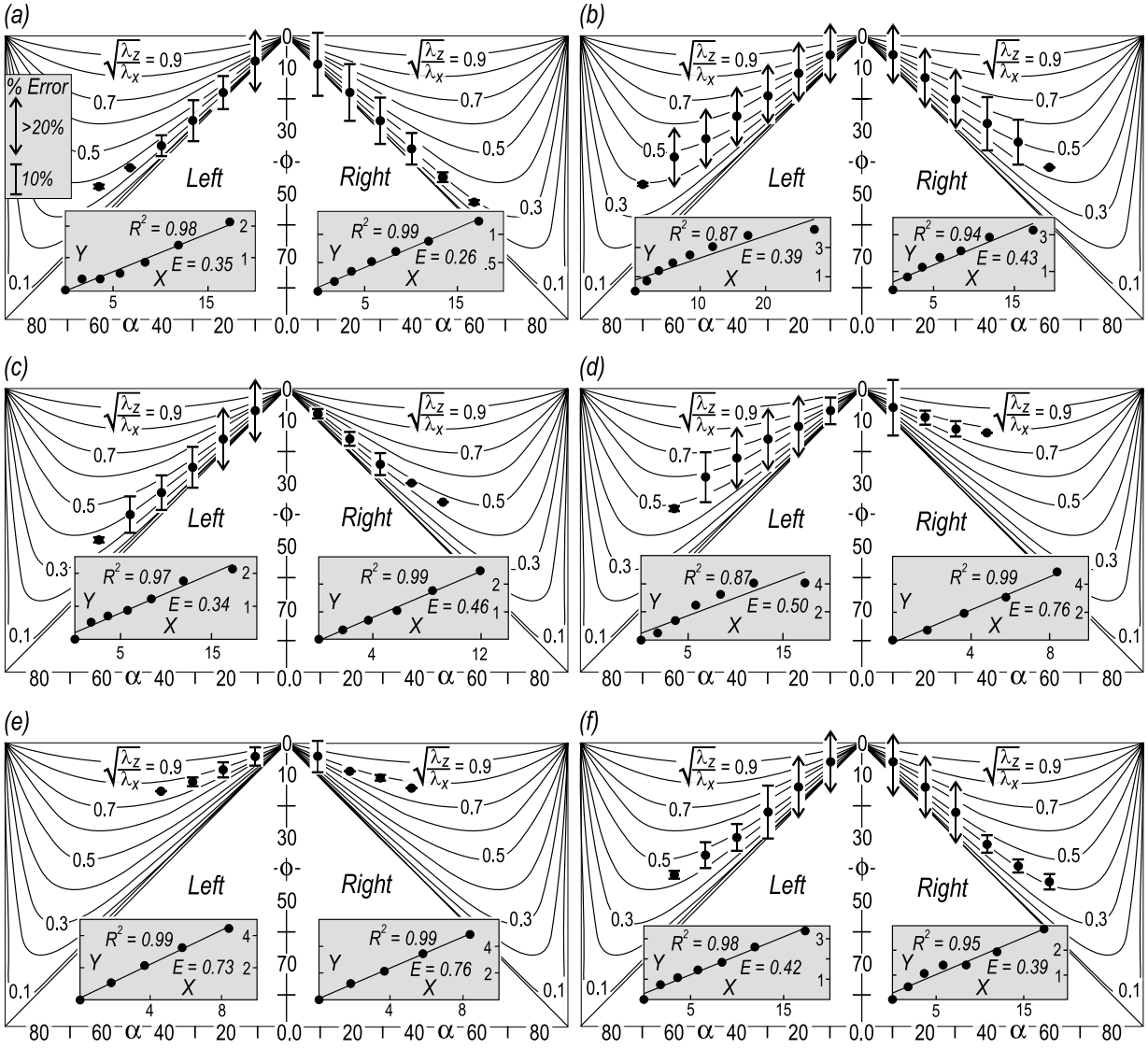

Fig. 6. (a)–(f) ϕ–α plots for left and right limbs of six folds shown in Fig. 3a–f, respectively. Error bars in all the figures are scaled off, as per the %-error scale, shown in (a). Insets show the best-fit lines, obtained by linear transformation of ϕ–α curves. $X = \tan\alpha$, $Y = \tan(\alpha - \phi)$. R^2—regression coefficient. E—expected value of $\sqrt{(\lambda_z/\lambda_x)}$ given by square root of slope of the best-fit line (Eq. (A4)).

$|90° - \delta|$, where δ is the angle between tangent and isogon at any given point on the destrained fold (inset in Fig. 8). This angular deviation is found to be $\leq 5°$ in about 90% of the total 68 measurements in the six-fold examples tested in this study (Fig. 8).

5. Conclusions

The destraining method developed in this article is relatively rapid, as it requires drawing of only two or three isogon–tangent pairs. It also obviates the need for measuring angles and thickness at several points on the folded surface. As the method does not require locating hinge points and drawing axial traces, it is also free from uncertainties that may arise due to these geometrical constructions. Whereas other methods only estimate flattening strain, our method also restores the pre-flattening shape of flattened parallel fold without any additional geometrical or numerical steps. The quick and easy restoration of the pre-flattening fold shape is useful because it facilitates estimation of the buckling strain under the condition of constant area deformation.

Acknowledgements

This work is funded by the Department of Science and Technology, Government of India (SR/S4/ES60/2003) to Deepak C. Srivastava and the Ministry of Human Resource Development Fellowship to Jyoti Shah. Erudite reviews from Peter Hudleston, Fernando Bastida and T.G. Blenkinsop are acknowledged gratefully.

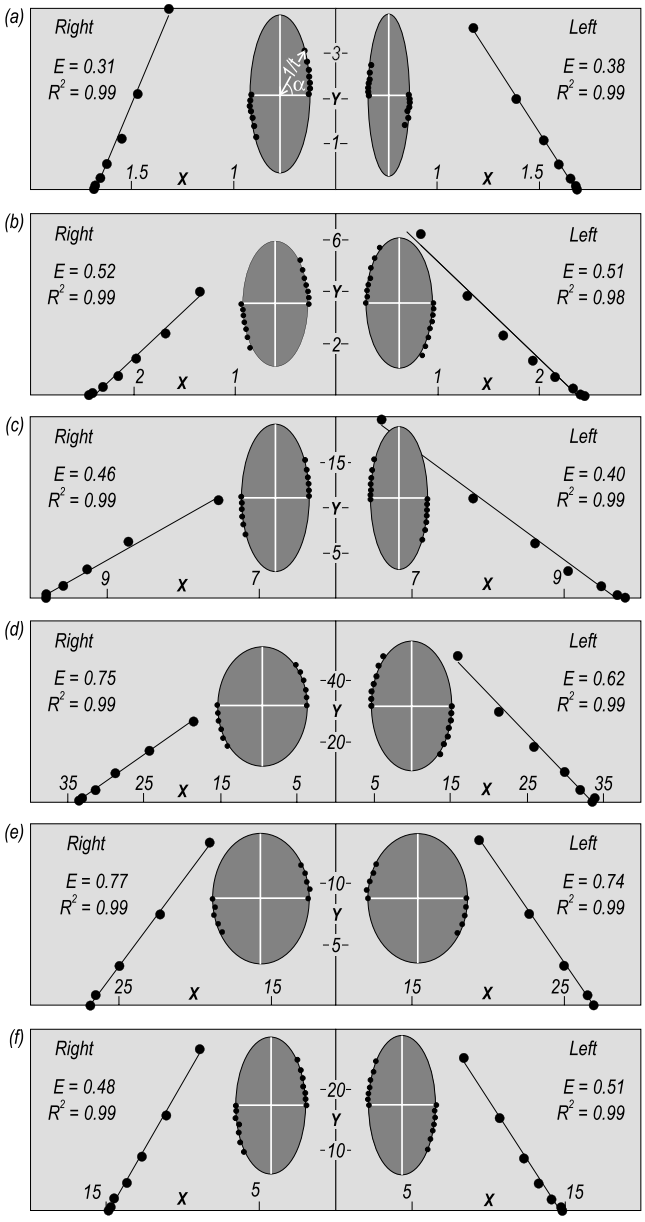

Fig. 7. (a)–(f) The best-fit lines (Eq. (A6)) through X–Y plots for right and left limbs of six folds shown in Fig. 3a–f, respectively. $X=\{(1/t)\cos\alpha\}^2$, $Y=\{(1/t)\sin\alpha\}^2$. E—expected value of axial ratio, $\sqrt{(\lambda_z/\lambda_x)}$, given by square root of slope of the best-fit lines. The best-fit ellipses, through the $1/t-\alpha$ polar plots, are shown in each case.

Appendix. Transformation of standard curves and ellipses into straight lines

For the estimation of flattening by curve matching, Ramsay (1967, p. 413) and Hudleston (1973a) give a set of $t'_\alpha-\alpha$ and ϕ–α curves corresponding to different values of $\sqrt{(\lambda_z/\lambda_x)}$ ratios. One main limitation of these graphical approaches is that curves for different magnitudes of flattening strain tend to merge with each other, particularly at low angles of the limb dip and small values of $\sqrt{(\lambda_z/\lambda_x)}$ ratio (Figs. 5 and 6). Another limitation, implicit in the curve matching procedures, is that the t'_α or ϕ data, corresponding to different angles of the limb dip (α) in a given fold, seldom fall on a unique curve (Figs. 5 and 6). The strain determination from visual best-fit matching with the standard curves is, therefore, qualitative and subjective.

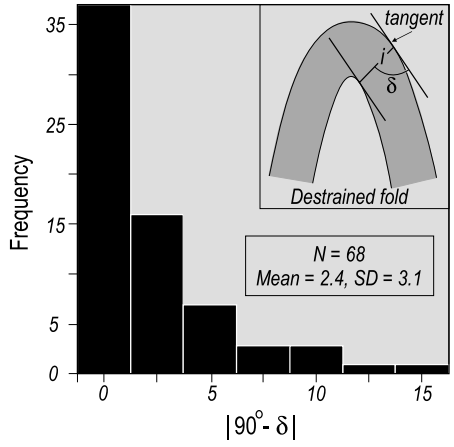

Fig. 8. Histogram showing errors in destraining method. δ—angle between tangent and isogon. N—number of observations. SD—standard deviation.

In order to eliminate the subjectivity in visual fitting, we transform the three equations that relate t'_α, ϕ and inverse thickness ($1/t$) to limb dip angle (α) in linear forms as follows:

$$(t'_\alpha)^2 = (\lambda_z/\lambda_x) + (1-\lambda_z/\lambda_x)\cos^2\alpha$$

(after Ramsay, 1967, p. 412) (A1)

By substituting $(t'_\alpha)^2 = Y$ and $\cos^2\alpha = X$, we can rearrange Eq. (A1) as:

$$Y = MX + C,$$

where $M = (1-\lambda_z/\lambda_x)$ and $C = \lambda_z/\lambda_x$. (A2)

As shown by Hudleston (1973a), the following relationship between ϕ and α

$$\tan(\alpha-\phi) = (\lambda_z/\lambda_x)\tan\alpha \quad \text{(A3)}$$

can also be rearranged in a linear form as:

$$Y = mX \quad \text{(A4)}$$

where $\tan(\alpha-\phi)=Y$, $\tan\alpha=X$ and $\lambda_z/\lambda_x=m$.

Similarly, the equation of ellipse, obtained in the inverse thickness method of Lisle (1992), can also be transformed into linear form as follows:

$$(x^2/a^2) + (y^2/b^2) = 1 \quad \text{(A5)}$$

$$Y = AX + B \quad \text{(A6)}$$

where $y^2=Y$, $x^2=X$, $-(b^2/a^2)=A$ and $b^2=B$.

These simple linear transformations of Eqs. (A1), (A3) and (A5) facilitate the drawing of the least square best-fit lines through the points on the graphs plotted between X and Y variables defined in Eqs. (A2), (A4) and (A6), respectively

Table 1
Comparison of the results obtained by application of different methods on the six folds shown in Fig. 3a–f. $\sqrt{(\lambda_z/\lambda_x)}$—axial ratio of the strain ellipse representing flattening

Example		$\sqrt{(\lambda_z/\lambda_x)}$ ratio obtained by different methods			
		$t'_\alpha - \alpha$ method	ϕ–α method	Inverse thickness method	Destraining method
Fold 1 (Fig. 3a)	Left limb	0.38	0.35	0.38	0.35
	Right limb	0.31	0.29	0.31	0.30
Fold 2 (Fig. 3b)	Left limb	0.54	0.39	0.51	0.53
	Right limb	0.54	0.43	0.52	0.50
Fold 3 (Fig. 3c)	Left limb	0.41	0.34	0.40	0.39
	Right limb	0.45	0.45	0.46	0.46
Fold 4 (Fig. 3d)	Left limb	0.62	0.50	0.62	0.61
	Right limb	0.74	0.76	0.75	0.77
Fold 5 (Fig. 3e)	Left limb	0.74	0.73	0.74	0.75
	Right limb	0.77	0.76	0.77	0.76
Fold 6 (Fig. 3f)	Left limb	0.51	0.42	0.51	0.50
	Right limb	0.48	0.39	0.48	0.49

(insets in Figs. 5–7). Fig. A1 shows a set of nine straight lines for λ_z/λ_x ratios, ranging from 0.1 to 0.9, that can be obtained from Eqs. (A2) and (A4), respectively.

Errors in the $t'_\alpha - \alpha$ and the ϕ–α methods are obtained in terms of %-error in $\sqrt{(\lambda_z/\lambda_x)}$ ratios for different α angles. This %-error equals $(|O-E|100)/E$, where O and E are the observed and the expected values of $\sqrt{(\lambda_z/\lambda_x)}$ ratios, respectively. The observed values (O) in the $t'_\alpha - \alpha$ and the ϕ–α methods are obtained by substituting the values of t'_α and ϕ for different α angles, in Eqs. (A1) and (A3), respectively. Similarly, the expected values (E) are given by the square root of the intercept of the best-fit line (Eq. (A2)) in the $t'_\alpha - \alpha$ method, and the square root of slope of the best-fit line (Eq. (A4)) in the ϕ–α method (insets in Figs. 5 and 6).

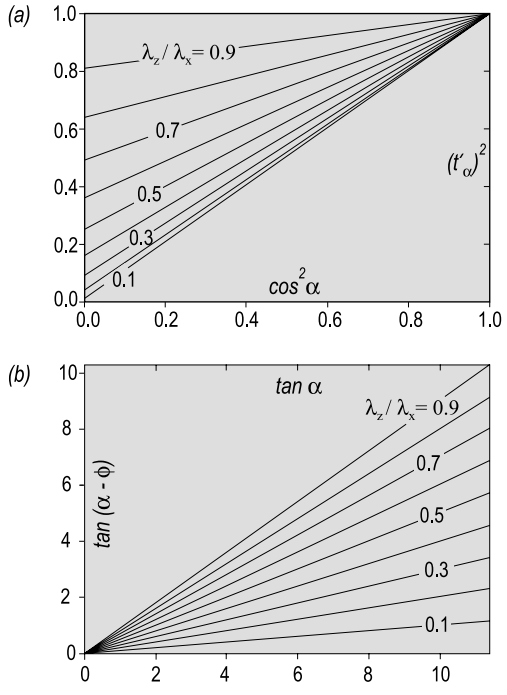

Fig. A1. (a) and (b) Straight line transformations of the $t'_\alpha - \alpha$ and the ϕ–α curves for λ_z/λ_x ratios from 0.1 to 0.9, respectively.

References

Bastida, F., Bobillo-Ares, N.C., Aller, J., Toimil, N.C., 2003. Analysis of folding by superposition of strain pattern. Journal of Structural Geology 25, 1121–1139.

Biot, M.A., 1961. Theory of folding of stratified viscoelastic media and its implication in tectonics and orogenesis. Geological Society of America Bulletin 72, 1595–1620.

Chatterji, A., 1987. Morphological distinction between buckling-and-flattening folds and flattened parallel folds. Indian Journal of Geology 59, 29–55.

Dietrich, H., 1969. Origin of cleavage in folded rocks. American Journal of Science 267, 155–165.

Ghosh, S.K., 1993. Structural Geology, Fundamentals and Modern Developments. Pergamon Press, England. 598pp.

Hudleston, P.J., 1973a. Fold morphology and some geometric implications of theories of fold development. Tectonophysics 16, 1–46.

Hudleston, P.J., 1973b. An analysis of 'single layer' folds developed experimentally in viscous media. Tectonophysics 16, 189–214.

Hudleston, P.J., 1973c. The analysis and interpretation of minor folds developed in the Moine rocks of Monar, Scotland. Tectonophysics 17, 89–132.

Lisle, R.J., 1992. Strain estimation from flattened buckled folds. Journal of Structural Geology 14, 369–371.

Ramberg, H., 1963. Strain distribution and geometry of folds. Bulletin of Geological Institute, University of Uppsala 42, 1–20.

Ramsay, J.G., 1962. The geometry and mechanics of formation of similar type folds. Journal of Geology 70, 309–327.

Ramsay, J.G., 1967. Folding and Fracturing of Rocks. McGraw Hill, New York. 568pp.

Srivastava, D.C., Srivastava, P., 1988. The modification of parallel folds by progressive shearing parallel to the axial plane. Tectonophysics 156, 167–173.

Srivastava, H.B., 2003. Strain determination from concentric folds. Tectonophysics 364, 237–241.

Treagus, J.E., Treagus, S.H., 1981. Folds and strain ellipsoid: a general model. Journal of Structural Geology 3, 1–17.

Treagus, S.H., 1982. A new isogon-cleavage classification and its application to natural and model fold studies. Geological Journal 17, 49–76.